Crystal Structure of the Second Domain of the Human Copper Chaperone for Superoxide Dismutase[†,‡]

Audrey L. Lamb,[§] Amy K. Wernimont,[§] Robert A. Pufahl,[||] Thomas V. O'Halloran,[§,||] and Amy C. Rosenzweig*[,§,||]

Department of Biochemistry, Molecular Biology, and Cell Biology and Department of Chemistry, Northwestern University, Evanston, Illinois 60208

Received December 8, 1999; Revised Manuscript Received December 23, 1999

ABSTRACT: The human copper chaperone for superoxide dismutase (hCCS) delivers the essential copper ion cofactor to copper,zinc superoxide dismutase (SOD1), a key enzyme in antioxidant defense. Mutations in SOD1 are linked to familial amyotrophic lateral sclerosis (FALS), a fatal neurodegenerative disorder. The molecular mechanisms by which SOD1 is recognized and activated by hCCS are not understood. To better understand this biochemical pathway, we have determined the X-ray structure of the largest domain of hCCS (hCCS Domain II) to 2.75 Å resolution. The overall structure is closely related to that of its target enzyme SOD1, consisting of an eight-stranded β-barrel and a zinc-binding site formed by two extended loops. The first of these loops provides the ligands to a bound zinc ion, and is analogous to the zinc subloop in SOD1. The second structurally resembles the SOD1 electrostatic channel loop, but lacks many of the residues important for catalysis. Like SOD1 and yCCS, hCCS forms a dimer using a highly conserved interface. In contrast to SOD1, however, the hCCS structure does not contain a copper ion bound in the catalytic site. Notably, the structure reveals a single loop proximal to the dimer interface which is unique to the CCS chaperones.

Superoxide dismutases (SODs) catalyze the disproportionation of superoxide to hydrogen peroxide and dioxygen, a crucial reaction in cellular antioxidant defense, preventing oxidative damage of proteins, nucleic acids, and lipids. In eukaryotic cells, copper,zinc superoxide dismutase (SOD1),[1] a cytoplasmic, homodimeric enzyme, catalyzes this reaction via the redox cycling of a Cu(II) ion (*1*). The Cu(II) ion is located at the base of a channel lined by residues which guide the negatively charged substrate, superoxide, to the positively charged active site. A Zn(II) ion is linked to the catalytic Cu(II) ion by a bridging histidine residue (*2*−*4*). Recently, mutations in the gene for human SOD1 (hSOD1) have been linked to familial amyotrophic lateral sclerosis (FALS), a neurodegenerative disorder that is usually fatal within 5 years of the onset of symptoms (*5*, *6*). Characterization of several hSOD1 FALS mutations in transgenic mice are consistent with a gain-of-function activity that contributes to motor neuron degeneration (*7*). The biochemical basis of this gain-of-function activity is not understood, but may involve abnormal folding and aggregation of hSOD1 or aberrant oxidative chemistry catalyzed by the active-site copper ion (*8*−*11*).

Although SOD1 binds copper with high affinity in vivo and in vitro, copper insertion requires a copper chaperone protein, the copper chaperone for superoxide dismutase (CCS) (*12*−*14*). CCS, which is found in both yeast (yCCS) and humans (hCCS), belongs to an emerging family of metallochaperone proteins that function specifically in the intracellular delivery of metal ions (*15*). Other copper chaperone proteins (*16*, *17*) include yeast Atx1 (*15*, *18*, *19*) and its human homologue Hah1 (*20*, *21*), which shuttle copper to transport ATPases in the secretory pathway, and Cox17, which plays a role in the pathway for copper delivery to the mitochondria for incorporation into cytochrome *c* oxidase (*22*, *23*). Copper chaperones are necessary because intracellular free copper concentrations are maintained at exceedingly low levels (*13*). Copper delivery to yeast SOD1 (ySOD1) occurs via a direct interaction between yCCS and ySOD1 (*13*), but the molecular mechanisms of protein−protein recognition and metal ion transfer are not understood.

We recently reported the high-resolution crystal structure of yCCS (*24*). Structural, genetic, and biochemical studies reveal three functional domains (*25*). The N-terminal domain (Domain I) is structurally homologous to the metal-binding domains in Atx1 and other metal trafficking proteins and is believed to recruit cellular copper (*24*, *25*). The C-terminal domain (Domain III), which is disordered in the crystal structure, comprises 30 amino acid residues and is required

[†] This work was supported by NIH Grants GM58518 (to A.C.R.) and GM5411 (to T.V.O.), by grants from the ALS Association (to A.C.R. and T.V.O.), and by NIH NRSA Fellowships GM19973 (to A.L.L.) and DK09305 (to R.A.P.). The DND-CAT Synchrotron Research Center at the Advanced Photon Source is supported by the E. I. DuPont de Nemour & Co., The Dow Chemical Company, the NSF, and the State of Illinois.

[‡] Refined coordinates have been deposited in the Protein Data Bank with accession code 1DO5.

* To whom correspondence should be addressed. Phone: (847) 467-5301. Fax: (847) 467-6489. E-mail: amyr@nwu.edu.

[§] Department of Biochemistry, Molecular Biology, and Cell Biology.

[||] Department of Chemistry.

[1] Abbreviations: SOD1, Cu,Zn superoxide dismutase; FALS, familial amyotrophic lateral sclerosis; CCS, copper chaperone for superoxide dismutase; ySOD1, yeast Cu,Zn superoxide dismutase; hSOD1, human Cu,Zn superoxide dismutase; yCCS, yeast copper chaperone for superoxide dismutase; hCCS, human copper chaperone for superoxide dismutase; Atx1, antioxidant protein 1; ICP-AES, inductively coupled plasma atomic emission spectroscopy; ESI MS, electrospray ionization mass spectrometry; rms, root-mean-square.

10.1021/bi992822i CCC: $19.00
Published on Web 01/28/2000

for activation of ySOD1 (*25*). The middle domain (Domain II) exhibits a fold similar to that of its target enzyme, ySOD1, and may facilitate target recognition for copper delivery (*24*). Two structural features of yCCS Domain II are notable. First, two key loops which are present in yeast and human SOD1s, the zinc-binding loop and the electrostatic channel loop, are not found in yCCS. As a result, this domain of yCCS lacks the canonical metal-binding sites and active-site channel found in SOD1. Second, residues from Domain II interact to form a homodimer in the crystal, which closely resembles the SOD1 homodimer. A structure-based sequence alignment of yCCS, hCCS, ySOD1, and hSOD1 suggests that hCCS Domain II may not share all of these features (*24*). To define the structural similarities and differences in this family, we have determined the X-ray structure of hCCS Domain II.

EXPERIMENTAL PROCEDURES

Purification of hCCS. The gene for full-length hCCS was cloned into the expression vector pET24d (Novagen) and transformed into *Escherichia coli* strain BL21(DE3) (*26*). Transformed bacteria were grown in Luria Broth to an optical density at 600 nm of 0.6−0.8, and hCCS expression was induced with 0.5−1.0 mM IPTG. At the time of induction with IPTG, $CuSO_4$ and $ZnSO_4$ were added to the media, both to a final concentration of 200 μM. Purification was achieved by freeze−thaw extraction and precipitation with 25% ammonium sulfate. After dialysis into 50 mM Tris, pH 8.0, SDS−PAGE analysis indicated that the hCCS protein was >95% pure and had a molecular mass of ∼30 kDa. Purified material was concentrated to 7 mg/mL for crystallization and stored at −80 °C in 50 mM Tris, pH 8.0. Metal analysis by inductively coupled plasma atomic emission spectroscopy (ICP-AES) and a calibrated Bradford assay (*26*) indicated that hCCS contained 1.0 zinc ion and 0.2 copper ion/monomer of purified protein.

Crystallization and Data Collection. Crystallization of hCCS was carried out by the hanging drop method at 25 °C. Drops containing 1−2 μL of 7 mg/mL protein were mixed with equal volumes of a reservoir solution composed of 100 mM Mes, pH 6.5, and 12% PEG 20 000. After 7 days, clusters of very thin crystal plates appeared. The crystals belong to the space group *C*2 with unit cell dimensions $a = 118.7$ Å, $b = 67.0$ Å, $c = 89.0$ Å, and $\beta = 97.1°$. Single plates of approximate dimensions 0.01 × 0.1 × 0.2 mm were transferred to reservoir solution that also contained 20% ethylene glycol as a cryosolvent and immediately flash cooled at −160 °C. Diffraction to 2.7 Å resolution was observed using synchrotron radiation at the Dupont-Northwestern-Dow Collaborative Access Team (DND-CAT) beamline at the Advanced Photon Source, but the crystals were highly mosaic and the diffraction pattern was of poor quality. After crystal annealing by blocking the cold stream for 5 s, the mosaicity decreased significantly, and it was possible to collect a complete data set using a 2K × 2K Mar CCD detector (Table 1). The data were processed with DENZO and SCALEPACK (*27*).

Structure Determination. The structure was solved by molecular replacement with AMoRe (*28*) using data in the 8.0−4.0 Å resolution range. The ySOD1 dimer (*29*) (PDB accession number 1SDY) including side chains but no Cu(II) or Zn(II) ions was used as a search model. Rotation and translation searches yielded a clear solution with a correlation coefficient of 0.320 and an *R*-factor of 0.536. The map generated from this solution revealed a considerable amount of density not accounted for by the starting model. All attempts to model this density with an Atx1-like structural domain were unsuccessful. Using the program O (*30*), the side chains of the starting model were modified to fit the hCCS sequence and a partial polyalanine model was built into part of the remaining density. After rigid body and positional refinement with CNS (*31*), phases from this model were used to calculate a new map. This map quite clearly indicated that the unidentified density corresponded not to an Atx1-like domain but to a second SOD1-like dimer. Several cycles of model rebuilding, simulated annealing refinement, and individual *B*-value refinement with CNS yielded a final model consisting of two dimers of hCCS Domain II. Of the four monomers in these dimers, two are modeled as containing residues 87−234, one is modeled as containing residues 85−237, and the last is modeled with residues 84−237. Noncrystallographic symmetry restraints were imposed until the final cycles of refinement. In addition, 4 Zn(II) ions and 26 water molecules were modeled (Table 1). A Ramachandran plot generated with PROCHECK (*32*) shows that the current model exhibits good geometry with 81.7% of the residues in the most favored regions, 16.3% of the residues in the additionally allowed regions, and no residues in disallowed regions. Figures were generated using MOLSCRIPT (*33*), BOBSCRIPT (*34*), and RASTER3D (*35*). The dimer interfaces were analyzed using the Protein−Protein Interaction Server (www.biochem.ucl.ac.uk/bsm/PP/server).

Table 1: Data Collection and Refinement Statistics

data collection[a]	
resolution range (Å)	30.0−2.75
total observations	57 239
unique observations	17 387
completeness (%)[b]	96.5 (94.4)
R_{sym}[c]	0.080 (0.312)
I/σ	6.7 (2.5)
refinement	
resolution range (Å)	19.2−2.75
no. of reflections	14 376
R-factor[d]	0.229
R_{free}	0.284
no. of nonhydrogen protein atoms	4467
no. of solvent atoms	30
rms bond length (Å)	0.007
rms bond angles (deg)	1.4
avg *B* value (Å^2)	32.1

[a] Data collected at −160 °C using a 2K × 2K Mar CCD detector at the DND-CAT beamline at the Advanced Photon Source. Wavelength, 1.0 Å. [b] Values in parentheses are for the highest resolution shell: 2.83−2.75 Å. [c] $R_{sym} = \Sigma|I_{obs} - I_{avg}|/\Sigma I_{obs}$, where the summation is over all reflections. [d] *R*-factor $= \Sigma|F_{obs} - F_{calc}|/\Sigma F_{obs}$. Five percent of the reflections were reserved for calculation of R_{free}.

Determination of Protein Fragment Size. After discovering that only Domain II was present in the structure, crystals of hCCS were analyzed by SDS−PAGE and mass spectrometry. Crystals of hCCS dissolved in water and subjected to SDS−PAGE gave a single band corresponding to a molecular mass of 16−20 kDa, indicating that the crystals contained a fragment of hCCS rather than the full-length protein. Further analysis of dissolved crystals by electrospray ionization mass spectrometry (ESI MS) indicated that the

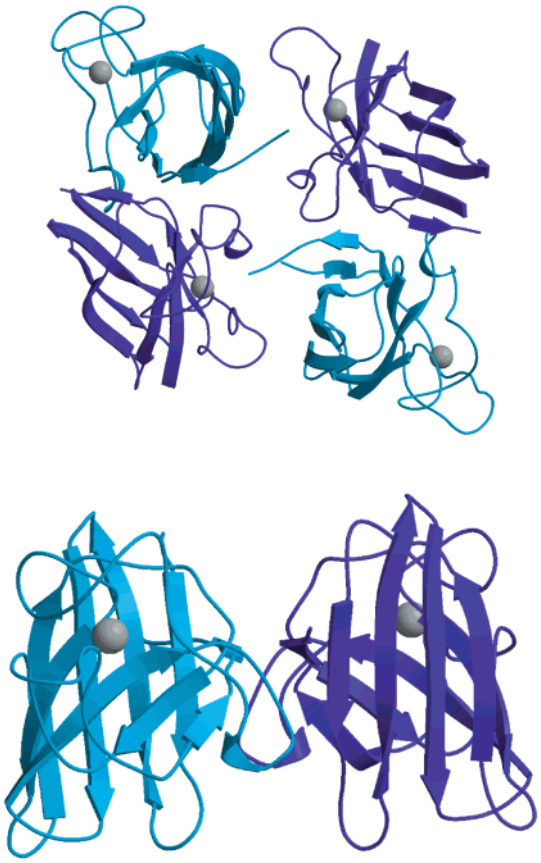

FIGURE 1: (a) The hCCS Domain II asymmetric unit. Monomers A (blue) and B (purple) form a dimer and monomers C (purple) and D (blue) form a dimer. (b) Dimer comprising monomers A and B. Each monomer houses one zinc ion (gray).

fragment mass was 16 511.8 ± 3 Da. Since the refined monomer model (residues 84−237) corresponds to a predicted mass of 16 272.0 Da, it is likely that a few amino acid residues at the termini are disordered and therefore not visible in the electron density map. Two reasonable possibilities are that residues 83 and 238 are disordered (predicted mass 16 513.3 Da) or that residues 238 and 239 are disordered (predicted mass 16 514.3 Da). We conclude that hCCS was proteolyzed in the crystallization drop, allowing Domain II alone to crystallize. These results are consistent with the observations that Domains I and II are quite distinct in the yCCS structure (*24*) and that all three domains have been separated in solution by proteolysis of yCCS (*25*) and hCCS (*26*).

RESULTS AND DISCUSSION

The structure of hCCS Domain II was determined by molecular replacement using the ySOD1 dimer as a search model (Table 1). The asymmetric unit contains four hCCS monomers which form two dimers (Figure 1). Monomer A interacts with monomer B, and monomer C interacts with monomer D. In addition to the two dimer axes, a noncrystallographic 2-fold axis relates monomer A to D and monomer B to C. A superposition of the Cα coordinates of monomers A and D gives an overall root-mean-square (rms) difference of 0.298 Å whereas the rms difference for monomers A and B is 0.431 Å. Several residues at the termini of monomers B and C are disordered, and the final model for these two monomers consists of residues 87−234. By contrast, residues 84−237 were modeled for monomer A, and residues 85−237 were modeled for monomer B. In addition, one Zn(II) ion per monomer and a total of 26 water molecules were included in the final model. The overall structure more closely resembles those of the target enzymes ySOD1 and hSOD1 (*4*, *5*, *29*, *36*) than that of the yeast chaperone yCCS (*24*). Each monomer comprises an eight-stranded antiparallel β-barrel of approximate dimensions 28 Å × 28 Å × 34 Å, with seven connecting loops.

A comparison of the loop regions with those in both hSOD1 and yCCS reveals several important features of the hCCS Domain II structure (Figures 2 and 3). Loop 4 is extended and has two domains, one analogous to the S−S subloop and the other to the zinc subloop in hSOD1 (Figure 2, panels a and b). In all cytoplasmic SOD1s, the S−S subloop houses a cysteine residue, Cys 57, which forms a disulfide bond with Cys 146 located on β strand 8 (*4*). This disulfide bridge stabilizes the tertiary structure in this region (*37*). In hCCS, the corresponding residues, Cys 141 and Cys 227, also form a disulfide bond. Interestingly, a third cysteine residue is located adjacent to the disulfide bridge in hCCS, Cys 144. The sulfur atom of Cys 144 is ∼5 Å from the sulfur atom of Cys 141 and ∼4 Å from the sulfur atom of Cys 227. In hSOD1, the corresponding residue is an alanine, Ala 60. None of these three cysteine residues are conserved in yCCS, although the loop is present. Cys 141 and Cys 227 are replaced by hydrophobic residues, Val 143 and Leu 212, and Cys 144 is replaced by a threonine, Thr 146 (Figure 3).

The second part of loop 4 is similar to the zinc subloop in SOD1 (Figure 2, panels a and b, gray) and provides the ligands to a bound metal ion. The identity of this metal ion was assigned as Zn(II) since elemental analysis of the full-length protein indicated the presence of 1.0 Zn(II) ion per monomer. The Zn(II) ion occupies the same site as the Zn(II) ion in SOD1 and is coordinated by His 147, His 155, His 164, and Asp 167 in a distorted tetrahedral geometry (Figure 2b, Figure 4). All four of these ligands are conserved between hCCS and SOD1 (Figure 2, panels a and b, and Figure 3). By contrast, yCCS does not contain a loop analogous to the zinc subloop and has no metal-binding sites in Domain II (Figure 2c, gray, Figure 3). A second potential metal-binding site corresponding to the SOD1 catalytic copper center is located adjacent to the zinc site in hCCS. In SOD1, the Cu(II) ion is coordinated by four histidine residues, three of which are conserved in hCCS (His 130, His 132, and His 147). In SOD1, the residue corresponding to hCCS His 147 bridges the copper and zinc ions. The fourth histidine residue is replaced with an aspartic acid in hCCS, Asp 201 (Figure 2, panels a and b, and Figure 3).

Contrary to predictions (*38*), a metal ion is not found in this second site in the hCCS structure. In monomers B and C, the second site contains no residual electron density. In monomers A and D, a small peak consistent with the presence of a water molecule is observed (Figure 4). This peak is within hydrogen-bonding distance of the ϵ nitrogen atom of His 147 and a side-chain oxygen atom of Asp 201. Since this peak is located ∼2 Å from the position of the Cu(II) ion in SOD1, it probably does not represent a low occupancy Cu(II) ion. Furthermore, the average distances from this peak to the ϵ nitrogen atom of His 132 and the δ nitrogen atom of His 130 are significantly longer than expected for primary coordination (>1.5 Å). In all four

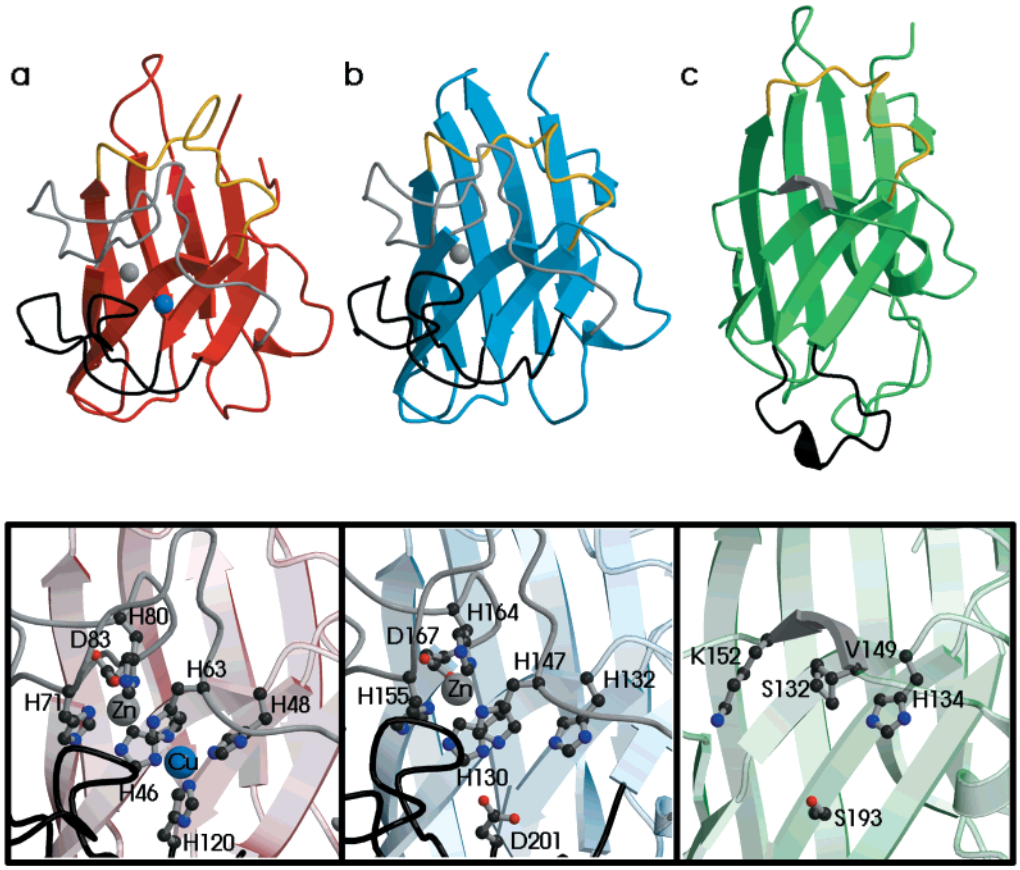

FIGURE 2: Comparison of hCCS Domain II (b) with hSOD1 (PDB accession code 1SPD) (a) and yCCS Domain II (PDB accession code 1QUP) (c). The gray loop regions correspond to hCCS loop 4 (hSOD1 zinc subloop), the black loop regions correspond to hCCS loop 7 (hSOD1 electrostatic channel loop), and the yellow loop regions correspond to hCCS loop 6 (hSOD1 Greek key loop). An enlargement of the metal binding sites, including coordinating amino acid residues, is shown for hSOD1 and hCCS. The corresponding region in yCCS is also shown. The Zn(II) ions are shown as gray spheres and the Cu(II) ion is shown as a blue sphere.

monomers, Asp 201 is not close enough to His 130 and His 132 to act as a fourth ligand to a metal ion. Since Asp 201 is located on β strand 7, the structure may not be able to accommodate the shift in position that would be required to bind metal ion. Hydrogen-bonding interactions linking the zinc-binding site and the second unoccupied site are conserved between hCCS and hSOD1. For example, Asp 205 connects the zinc ligand His 155 with His 130 via side-chain hydrogen bonds just as hSOD1 Asp 124 bridges the zinc ligand His 71 and the copper ligand His 46.

Loop 7 in hCCS (Figure 2b, black) corresponds to the electrostatic channel loop in SOD1 (Figure 2a, black), which together with the zinc subloop forms the active-site cavity. The loops in the two proteins are structurally similar, but a number of catalytically important residues are not conserved. In hSOD1, residues Glu 132, Glu 133, and Lys 136 play an important role in directing the long-range approach of the substrate, superoxide (*39*, *40*), to the active site. The corresponding residues in hCCS are hydrophobic, Pro 213, Leu 214, and Ile 217 (Figure 3). Other electrostatically important residues in hSOD1, including Asn 131, Thr 135, Glu 121, and Lys 122 (*4*), are replaced in hCCS by His 212, Lys 216, Glu 202, and Gly 203. It is noteworthy, however, that one critical residue in hSOD1, Arg 143, is conserved in hCCS, Arg 224. This residue functions to orient and stabilize superoxide at the catalytic copper site (*3*, *41*). SOD activity is observed in yeast that lack SOD1, but express a mutant hCCS in which Asp 201 is replaced with a histidine residue to mimic the SOD1 copper site (*42*). This finding is consistent with the structure in that the active-site cavity is present along with this catalytically important arginine residue. Furthermore, the absence of other electrostatically significant residues likely explains why the mutant hCCS is not as active as wild-type SOD1 (*42*). In yCCS, the loop corresponding to the electrostatic channel loop is shorter in length and is in a completely different position than the analogous loops in hCCS and SOD1 (Figure 2c, black, Figure 3). It interacts with loop 1, which is significantly longer in yCCS than in hCCS (Figure 3).

Although hCCS Domain II is more similar structurally to hSOD1 than to yCCS Domain II, there is one key difference. Loop 6 of hCCS (Figure 2b, yellow, Figure 3) more closely resembles the analogous loop in yCCS (Figure 2c, yellow) than that in hSOD1 (Figure 2a, yellow). Loop 6 in hCCS and the corresponding loop in yCCS are shorter in length than their SOD1 counterparts and both house a single, solvent exposed tryptophan. This residue, Trp 191 in hCCS or Trp 183 in yCCS, is found in place of a four amino acid sequence in SOD1 (Figure 3). One consequence of replacing four residues in this loop with a single residue is that two arginine residues, Arg 196 and Arg 232, become less buried, creating a surface patch of positive charge near the dimer interface. One of these residues, Arg 196, is conserved in SOD1, whereas the other, Arg 232, is only present in the two chaperones. As the only structural element unique to the CCS proteins, loop 6 could be important in metal delivery, perhaps

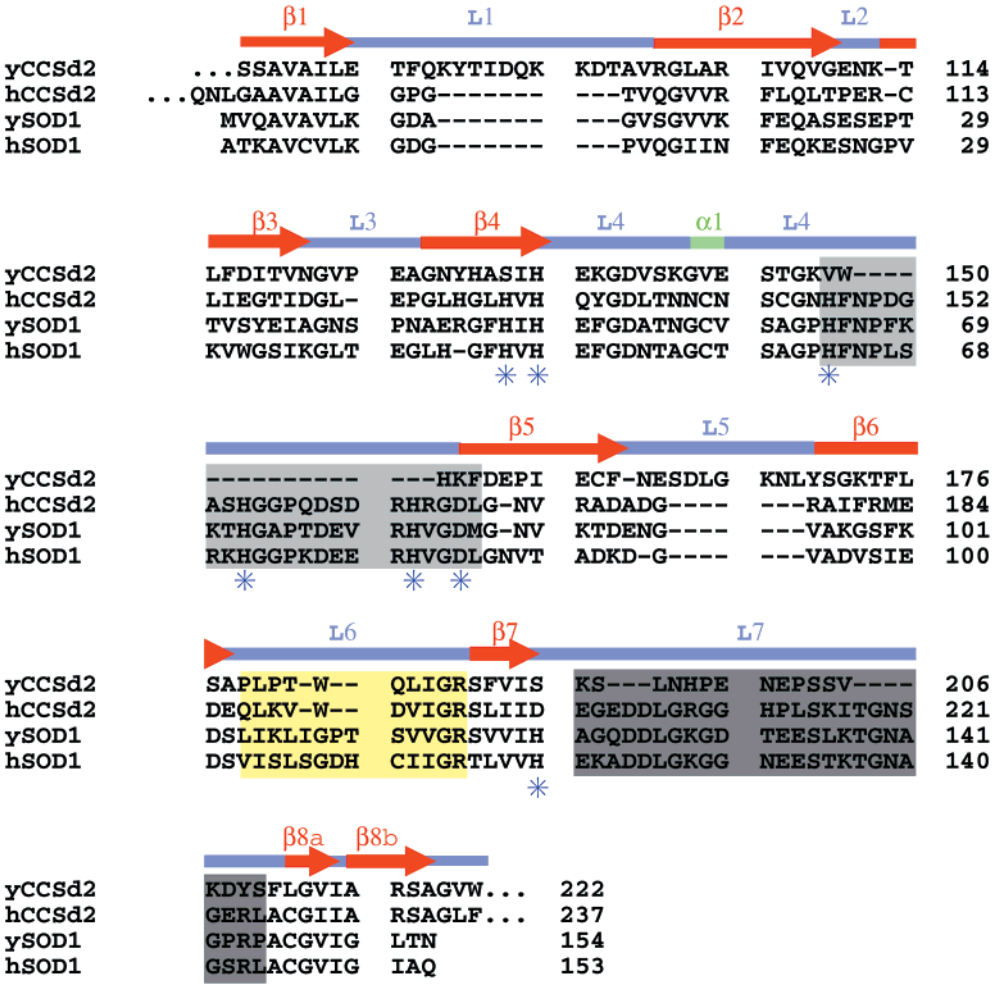

FIGURE 3: Structure-based sequence alignment of hCCS Domain II with yCCS Domain II, hSOD1, and ySOD1. The positions of the hCCS Domain II secondary structure elements are shown above the sequence alignment. β-strands are shown as red arrows and loop regions are shown as purple lines. In all four sequences, residues corresponding to hCCS loop 4 are shaded light gray, residues corresponding to hCCS loop 7 are shaded dark gray, and residues corresponding to hCCS loop 6 are shaded yellow. Metal ligands are denoted by blue asterisks.

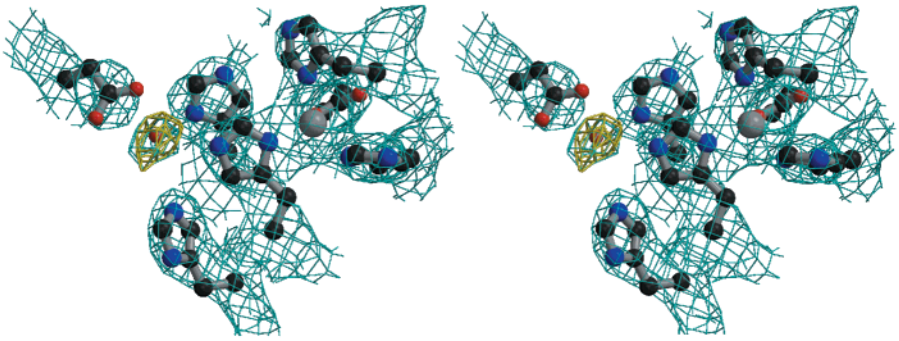

FIGURE 4: Stereoview of the final 2.75 Å resolution $2F_o - F_c$ electron density map at the zinc binding site in hCCS Domain II (blue, contoured at 1σ). The $F_o - F_c$ map showing the water molecule in monomers A and D is superimposed (yellow, contoured at 2σ).

facilitating recognition of and docking with SOD1. This loop might also interact with one of the other CCS domains, perhaps Domain III.

One of the outstanding features of the yCCS structure is that the dimer interface is highly conserved both structurally and sequentially between yCCS and ySOD1 (*24*). These interfaces involve four strong main-chain hydrogen bonds and a number of hydrophobic residues. As anticipated from a structure-based sequence alignment (*24*), the same interactions occur in hCCS. Residues Gly 135, Gly 195, and Arg 232 form the main-chain hydrogen bonds, and hydrophobic residues Val 90, Ile 92, Val 102, Gly 135, Leu 137, Ile 194, Gly 195, Ile 229, Ala 231, and Ala 234 provide additional subunit contacts. The yCCS counterpart to Arg 232 is also an arginine residue, whereas the corresponding residue is a leucine in ySOD1 and an isoleucine in hSOD1 (Figure 3). This arginine residue is located in close proximity to Arg 196, which is invariant in both chaperones and SOD1s. As suggested for yCCS, the presence of these two positively charged residues might render the CCS dimer less stable than the SOD1 dimer (*24*). A third charged residue located at the yCCS dimer interface, Lys 136, is a tyrosine, Tyr 134, in

hCCS, however. Mutation of the corresponding residue in hSOD1, a phenylalanine, to a glutamic acid results in the formation of a stable monomer (*43*). The mean change in accessible surface area (ΔASA) per hCCS monomer (*44*) upon dimer formation is 740 Å^2, which is somewhat larger than the ΔASAs calculated for yCCS (680 Å^2), ySOD1 (622 Å^2) (*24*), and hSOD1 (658 Å^2) (PDB accession code 1SPD).

Since yCCS Domain II does not have either a copper- or a zinc-binding site and hCCS Domain II does not readily bind copper, one probable function of this domain is recognition of the target enzyme SOD1 and, more specifically, orientation of the copper donor and acceptor sites in the two proteins. Protein−protein complex formation can be envisioned in several ways. Since both yCCS and hCCS crystallize as dimers with interfaces large enough for stable dimer association, it is reasonable that homodimeric chaperone might interact with homodimeric target, forming a tetramer and facilitating metal ion transfer to both subunits of SOD1 simultaneously. In support of this model, gel filtration experiments show that hCCS does not exist as a monomer in solution under any conditions (*26*). Although yCCS is a monomer in the apo form, it exists as a mixture of monomers and dimers in the presence of copper (*25*). Alternatively, monomeric chaperone could interact with monomeric SOD1, exploiting the conserved dimer interface to form a heterodimer for metal ion insertion. Heterodimer formation has been observed for different isoforms of SOD1 from the same organism (*45*) as well as for SOD1s from quite distantly related organisms (*46*). Finally, the possibility that yCCS and hCCS dock via different mechanisms cannot be eliminated, although this seems unlikely since hCCS can rescue growth of yCCS deletion mutants in yeast (*12*). A detailed understanding of the CCS−SOD1 interaction awaits further biochemical analysis and crystallographic characterization of the protein−protein complex. Knowledge of the structural and mechanistic aspects of hCCS function will facilitate the design of inhibitors of the SOD1 activation pathway. Since SOD1-null mice are viable (*47*), such an approach may prove useful in the development of new FALS therapeutics.

ACKNOWLEDGMENT

We thank E. Ma for excellent technical assistance, V. Culotta and J. Gitlin for helpful discussions and plasmids, T. Rae and A. Torres for valuable advice, and J. Quintana, D. Keane, and Z. Wawrzak for assistance with data collection.

REFERENCES

1. McCord, J. M., and Fridovich, I. (1969) *J. Biol. Chem. 244*, 6049−6055.
2. Tainer, J. A., Getzoff, E. D., Beem, K. M., Richardson, J. S., and Richardson, D. C. (1982) *J. Mol. Biol. 160*, 181−217.
3. Getzoff, E. D., Tainer, J. A., Weiner, P. K., Kollman, P. A., Richardson, J., and Richardson, D. C. (1983) *Nature 306*, 287−290.
4. Bordo, D., Djinovic, K., and Bolognesi, M. (1994) *J. Mol. Biol. 238*, 366−386.
5. Deng, H.-X., Hentati, A., Tainer, J. A., Iqbal, Z., Cayabyab, A., Hung, W.-Y., Getzoff, E. D., Hu, P., Herzfeldt, B., Roos, R. P., Warner, C., Deng, G., Soriano, E., Smyth, C., Parge, H. E., Ahmed, A., Roses, A. D., Hallewell, R. A., Pericak-Vance, M. A., and Siddique, T. (1993) *Science 261*, 1047−1051.
6. Rosen, D. R., et al. (1993) *Nature 362*, 59−62.
7. Gurney, M. E., Pu, H., Chiu, A. Y., Canto, M. C. D., Polchow, C. Y., Alexander, D. D., Caliendo, J., Hentati, A., Kwon, Y. W., Deng, H.-X., Chen, W., Zhai, P., Sufit, R. L., and Siddique, T. (1994) *Science 264*, 1772−1775.
8. Beckman, J. S., Carson, M., Smith, C. D., and Koppenoll, W. H. (1993) *Nature 364*, 584.
9. Wiedau-Pazos, M., Goto, J. J., Rabizadeh, S., Gralla, E. B., Roe, J. A., Lee, M. K., Valentine, J. S., and Bredesen, D. E. (1996) *Science 271*, 515−518.
10. Siddique, T., Nijhawan, D., and Hentati, A. (1997) *J. Neural Transm. 49*, 219−233.
11. Wong, P. C., Rothstein, J. D., and Price, D. L. (1998) *Curr. Opin. Neurobiol. 8*, 791−799.
12. Culotta, V. C., Klomp, L. W. J., Strain, J., Casareno, R. L. B., Krems, B., and Gitlin, J. D. (1997) *J. Biol. Chem. 272*, 23469−23472.
13. Rae, T. D., Schmidt, P. J., Pufahl, R. A., Culotta, V. C., and O'Halloran, T. V. (1999) *Science 284*, 805−808.
14. Gamonet, F., and Lauquin, G. J. (1998) *Eur. J. Biochem. 251*, 716−723.
15. Pufahl, R. A., Singer, C. P., Peariso, K. L., Lin, S.-J., Schmidt, P., Culotta, V. C., Penner-Hahn, J. E., and O'Halloran, T. V. (1997) *Science 278*, 853−856.
16. Valentine, J. S., and Gralla, E. B. (1997) *Science 278*, 817−818.
17. Poulos, T. L. (1999) *Nat. Struct. Biol. 6*, 709−711.
18. Lin, S., Pufahl, R., Dancis, A., O'Halloran, T. V., and Culotta, V. C. (1997) *J. Biol. Chem. 272*, 9215−9220.
19. Rosenzweig, A. C., Huffman, D. L., Hou, M. Y., Wernimont, A. K., Pufahl, R. A., and O'Halloran, T. V. (1999) *Structure 7*, 605−617.
20. Klomp, L. W. J., Lin, S.-J., Yuan, D. S., Klausner, R. D., Culotta, V. C., and Gitlin, J. D. (1997) *J. Biol. Chem. 272*, 9221−9226.
21. Hung, I. H., Casareno, R. L. B., Labesse, G., Matthews, F. S., and Gitlin, J. D. (1998) *J. Biol. Chem. 273*, 1749−1754.
22. Glerum, D. M., Shtanko, A., and Tzagoloff, A. (1996) *J. Biol. Chem. 271*, 14504−14509.
23. Srinivasan, C., Posewitz, M. C., George, G. N., and Winge, D. R. (1998) *Biochemistry 37*, 7572−7577.
24. Lamb, A. L., Wernimont, A. K., Pufahl, R. A., O'Halloran, T. V., and Rosenzweig, A. C. (1999) *Nat. Struct. Biol. 6*, 724−729.
25. Schmidt, P. J., Rae, T. D., Pufahl, R. A., Hamma, T., Strain, J., O'Halloran, T. V., and Culotta, V. C. (1999) *J. Biol. Chem. 274*, 23719−23725.
26. Rae, T. D., Pufahl, R. A., and O'Halloran, T. V. Unpublished results.
27. Otwinowski, Z., and Minor, W. (1997) *Methods Enzymol. 276*, 307−326.
28. Collaborative Computational Project, Number 4 (1994) *Acta Crystallogr., Sect. D 50*, 760−763.
29. Djinovic, K., Gatti, G., Coda, A., Antolini, L., Pelosi, G., Desideri, A., Falconi, M., Marmocchi, F., Rotilio, G., and Bolognesi, M. (1992) *J. Mol. Biol. 225*, 791−809.
30. Jones, T. A., Zou, J.-Y., Cowan, S. W., and Kjeldgaard, M. (1991) *Acta Crystallogr., Sect. A 47*, 110−119.
31. Brünger, A. T., Adams, P. D., Clore, G. M., DeLano, W. L., Gros, P., Grosse-Kunstleve, R. W., Jiang, J.-S., Kuszewski, J., Nilges, M., Pannu, N. S., Read, R. J., Rice, L. M., Simonson, T., and Warren, G. L. (1998) *Acta Crystallogr., Sect. D 54*, 905−921.
32. Laskowski, R. A. (1993) *J. Appl. Crystallogr. 26*, 283−291.
33. Kraulis, P. J. (1991) *J. Appl. Crystallogr. 24*, 946−950.
34. Esnouf, R. M. (1997) *J. Mol. Graphics 15*, 132−134.
35. Merritt, E. A., and Bacon, D. J. (1997) *Methods Enzymol. 277*, 505−524.
36. Parge, H. E., Hallewell, R. A., and Tainer, J. A. (1992) *Proc. Natl. Acad. Sci. U.S.A. 89*, 6109−6113.
37. Abernethy, J. L., Steinman, H. M., and Hill, R. L. (1974) *J. Biol. Chem. 249*, 7339−7344.
38. Falconi, M., Iovino, M., and Desideri, A. (1999) *Structure 7*, 903−908.

39. Getzoff, E. D., Cabelli, D. E., Fisher, C. L., Parge, H. E., Viezzoli, M. S., Banci, L., and Hallewell, R. A. (1992) *Nature 358*, 347−351.
40. Fisher, C. L., Cabelli, D. E., Hallewell, R. A., Beroza, P., Lo, T. P., Getzoff, E. D., and Tainer, J. A. (1997) *Proteins 29*, 103−112.
41. Fisher, C. L., Cabelli, D. E., Tainer, J. A., Hallewell, R. A., and Getzoff, E. D. (1994) *Proteins 19*, 24−34.
42. Schmidt, P. J., Ramos-Gomez, M., and Culotta, V. C. (1999) *J. Biol. Chem. 274*, 36952−36956.
43. Bertini, I., Piccioli, M., Viezzoli, M. S., Chiu, C. Y., and Mullenbach, G. T. (1994) *Eur. J. Biophys. 23*, 167−176.
44. Jones, S., and Thornton, J. M. (1996) *Proc. Natl. Acad. Sci. U.S.A. 93*, 13−20.
45. Capo, C. R., Polticelli, F., Calabrese, L., Schinina, M. E., Carri, M. T., and Rotilio, G. (1990) *Biochem. Biophys. Res. Commun. 173*, 1186−1193.
46. Tegelström, H. (1975) *Hereditas 81*, 185−198.
47. Reaume, A. G., Elliott, J. L., Hoffman, E. K., Kowall, N. W., Ferrante, R. J., Siwek, D. F., Wilcox, H. M., Flood, D. G., Beal, M. F., Brown, R. H., Jr., Scott, R. W., and Snider, W. D. (1996) *Nat. Genet. 13*, 43−47.

BI992822I